Supplement of Solid Earth, 17, 573–600, 2026
https://doi.org/10.5194/se-17-573-2026-supplement

Solid Earth Open Access EGU

Supplement of

On the criticality of return flows in viscous accretionary wedges and its implications for deep-crustal exhumation in subduction zones

Ayan Patsa and Nibir Mandal

Correspondence to: Nibir Mandal (nibir.mandal@jadavpuruniversity.in)

Supplement

S1. Control of viscosity ratio on the dynamic pressure inside wedge

The corner flow theory presented in the main text (section 2), suggest that a wedge generates a dynamic pressure (P_d) field at its narrowing end (Fig. 1c), which serves as the driving force for the characteristic return flow. In tectonic settings with slab-parallel subduction, high dynamic pressures localize preferentially near the tip of the wedge and its overriding wall, as shown in Figure S1. This results in strong negative upward dynamic pressure gradients along the wedge, which forces materials to flow upward beneath the roof of the wedge. Our generalized corner flow model predicts a positive correlation of the P_d magnitude with the viscosity ratio (μ_r) between the overriding plate (OP) and the wedge, increasing consistently as μ_r rises. The dynamic pressure. At μ_r =10, the system hardly generates any dynamic pressure gradient along the wedge (Fig. S1 c), and the P_d-gradient across the wedge tends to deflect part of the return flow towards the overriding wall (Fig. 4c in the main text).

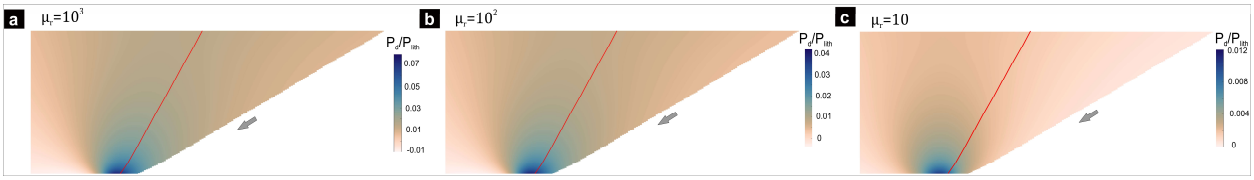

Fig. S1: Plot of normalized dynamic pressure (P_d) with varying μ_r. Arrows indicate slab-parallel subduction direction. $\mu_l = 10^{19}$ Pa s. $\theta_l = 30°$.

Slab advance motion during subduction contributes to the buildup of additional dynamic pressure at the base of the wedge and along the wall (Fig. S2 a-i, ii). For moderate μ_r (= 10^2), such a pressure field sets in return flows in both the wedge and its wall (Fig. 5d-i in the main text). In contrast, slow slab rollback ($\phi < \sim 2\theta_l/3$ or rigid OP) generates negative P_d due to bulk extension across the wedge, which counteracts the positive P_d produced by the wedge's taper geometry. Ultimately, the wedge fails to develop any significant dynamic pressure in a slow slab-rollback subduction setting (Figure S2 b-i, ii). Large slab rollback rates ($\phi > \sim 2\theta_l/3$) lower dynamic pressure and make it negative (Figure S2 b-i, ii). Such negative pressures 'draw in' the wedge materials towards the bottom in facilitating the burial of wedge materials at high rates, which locally exceed the subduction velocity (see Fig. 5c-i, f-i in the main text).

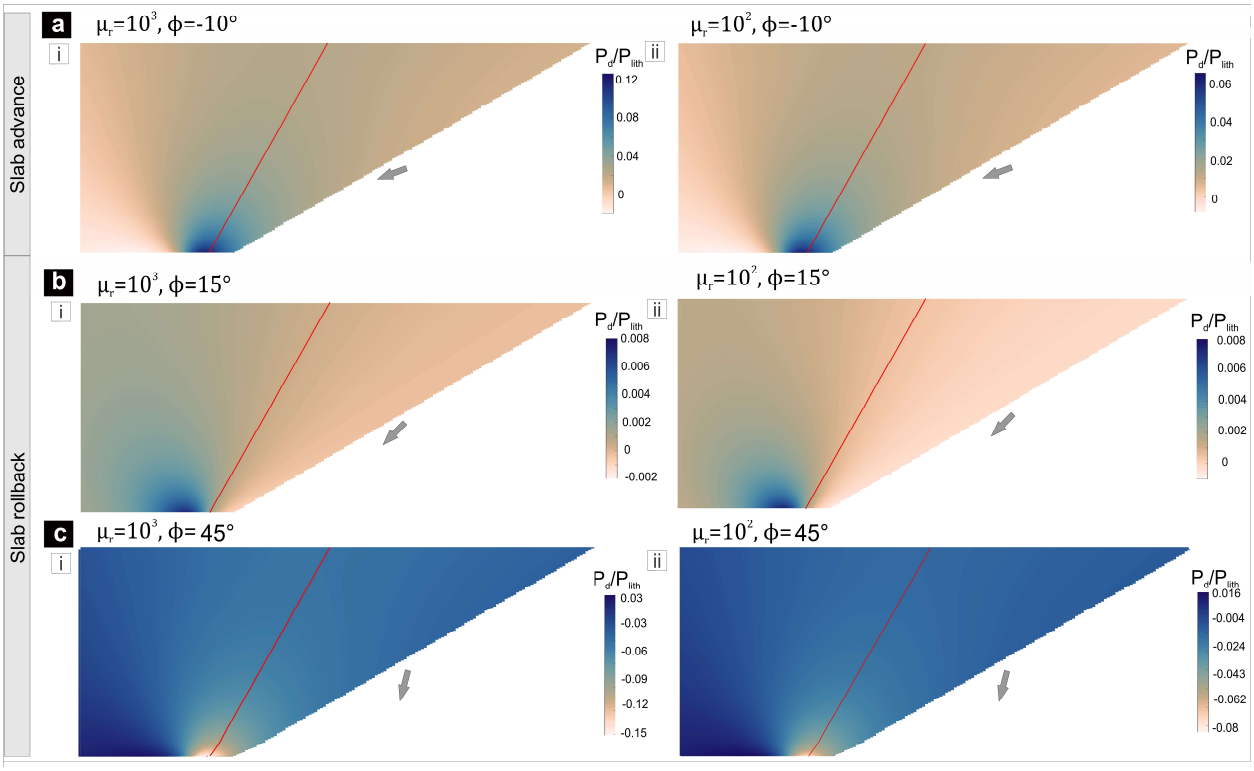

Fig. S2: Plot of normalized dynamic pressure (P_d) as a function of ϕ, and μ_r. $\mu_l = 10^{19}$ Pa s. $\theta_l = 30°$. P_{lith} is calculated assuming the overburden density as 2800 kg/m^3.

S2. Shear flows in accretionary wedges

For the model boundary conditions considered in our theoretical analysis, accretionary wedges accommodate deformation mostly by simple shear, although the sense of shearing can vary across the wedge, depending on the parametric conditions. The varying kinematic patterns are shown as a function of ϕ, θ_l, and μ_r in Fig. 12 in the main text. Three distinct modes of deformation can be recognized in the field diagram. The central part of the diagram defines a field of no shear reversal. For a low slab rollback velocity (i.e., low positive ϕ), the wedge shows no shear reversal unless the wedge taper angle is significantly large. The central field is bounded by two lines, the locus of which varies with μ_r. The field of no shear reversal widens with decreasing μ_r. To the left and right of this field, the shear sense reverses in the upper (i.e., near the OP) and lower (i.e., near the SP) regions of the wedge, respectively. The variation in the wedge kinematics results due to the complex interplay between the slab-driven Couette flow and the dynamic pressure-driven Poiseuille flow (Grujic et al., 2002; Mancktelow, 1995). The relative dominance of these two flows determines the pattern of shear within the wedge. For high μ_r, slab-parallel subduction or those

accompanied by slab advance or extremely slow slab rollback, develops large overpressures in the region close to the wedge tip (Fig. 13 in the main text), which facilitates the Poiseuille flows. In such a situation, the slab-driven shear induces clockwise vorticity throughout the wedge, whereas the pressure-driven flow induces clockwise (thrust-sense) and anticlockwise (normal-sense) vorticity in the lower and upper segments of the wedge, respectively. The lower part of the wedge thus undergoes thrust shear, whereas the pressure-driven flows creates normal shearing in the upper part of the wedge. On the other hand, for high μ_r, large rollback velocities (i.e., high ϕ) induce tectonic underpressure, resulting in a negative pressure gradient towards the tip that creates Poiseuille flows with downward velocity. Such conditions lead to localization of normal and thrust shearing in the lower and upper parts of the wedge, respectively. For low rollback velocities, the wedge develops gentle (positive or negative) dynamic pressure gradients, and the Couette flow dominates over the Poiseuille flow, as the negative P_d due to slab rollback is compensated by the positive P_d due to subduction (section S1). Such a dynamic condition favours the Couette flows, which give rise to thrust-sense shearing throughout the wedge. Wide wedges with large θ_I show weak effects of slab migration (advance or rollback) on the generation of dynamic pressures in them. This condition favors the occurrence of positive P_d, and shear reversal within a wider wedge (bi-vergent wedge), even for relatively high ϕ values (Fig. 12). When μ_r is low, for subduction, with or without slab migration (advance or rollback), the direction of maximum P_d-gradient is not along the wedge, but towards the OP (Fig. S1c). The Poiseuille flows induces significant deformations in the overriding plate, but not much effective in the wedge deformations. Low μ_r conditions thus facilitates thrust-sense shearing in the wedge. This explains the occurrence of a wider field of 'no shear reversal' for lower μ_r.

S3. Laboratory model experiments: velocity boundary conditions

The laboratory model setup consisted of three rigid buttresses, driven by two step-up motors, used differently in different sets of experiments to simulate slab-parallel subduction, slab advance, and slab rollback within the wedge (see Fig. 7 of the main text). For shearing, buttress 1 was driven to pull a plastic sheet along the wedge base at a rate of 0.7 mm/min. In another set of experiments, the plastic sheet had an along-base velocity (0.7 mm/min), coupled with a horizontal movement of buttress 2 that produced an across-wedge shortening velocity (0.15

mm/min). The two motions together simulated a condition of subduction at an angle (ϕ = -8°) to the wedge base. For the third set of experiments, a basal buttress, attached to step-up motor 2 by buttress 3, was placed at the base of the deformable wall (Figure 7 of the main text). This model configuration allowed the buttress 1 to tangentially move the plastic sheet along the wedge base (at 0.7 mm/min), as well as the deformable wall to move away (at 0.35 mm/min) from the wedge. This kinematic setup replicates a slab rollback kinematics with the movement direction at an angle to the wedge base (ϕ = 30°) away from the deformable wall in a reference frame fixed to the basal buttress. The velocity boundary conditions of the different sets of experiments are summarized below in Table S1.

Table S1. Imposed velocity boundary conditions for different sets of experiments.

Experiment	Buttress 1	Buttress 2	Basal buttress
Slab-parallel subduction	0.7 mm/min	0	0
Slab advance	0.7 mm/min	0.15 mm/min	0
Slab rollback	0.7 mm/min	0	0.35 mm/min

S4: Flow patterns in wedges: Whole laboratory model snaps

Analogue model results, presented in section 4 of the main text (Fig. 8, 9), focuses on the wedge kinematics in the bottom 20 km of the wedge. In this section, we provide experimental model photographs showing the velocity patterns in the whole 40 km thick model wedge (Fig. S3, S4). During the initial periods, high μ_r models produce effective return flows for slab-parallel subduction, and slab advance kinematics (Fig. S3 a-i, b-i). In contrast, low μ_r causes the return flow to significantly deflect towards the overriding plate (Fig. S4 a-i, b-i). Slab rollback kinematics largely facilitate burial of wedge materials and progressive subsidence of the wedge (Fg. S3 c-i, S4 c-i)

During subduction, at any instant, materials are buried at the maximum velocity in proximity to the moving wall. With progressive deformation, the wedge thus develops significant upper surface topographic slope at the front (see Fig. S3 a-ii, b-ii, c-ii; Fig. S4 a-ii, b-ii, c-ii). This topography results in gravity-driven (sub)-horizontal flow of materials from the rear to the

frontal parts of the wedge, more importantly close to the upper surface. The gravitational flows begin to modify the wedge kinematics even in the early stage of the experimental run. In natural subduction zones, different syntectonic processes, such as sedimentation, and erosion can, however, smoothen out the topographic slope, and suppress the gravity-driven flows (see section S5). In such cases, the first-order velocity field within the wedge will continue to follow the flow pattern predicted by the CF theory, as presented in the next section.

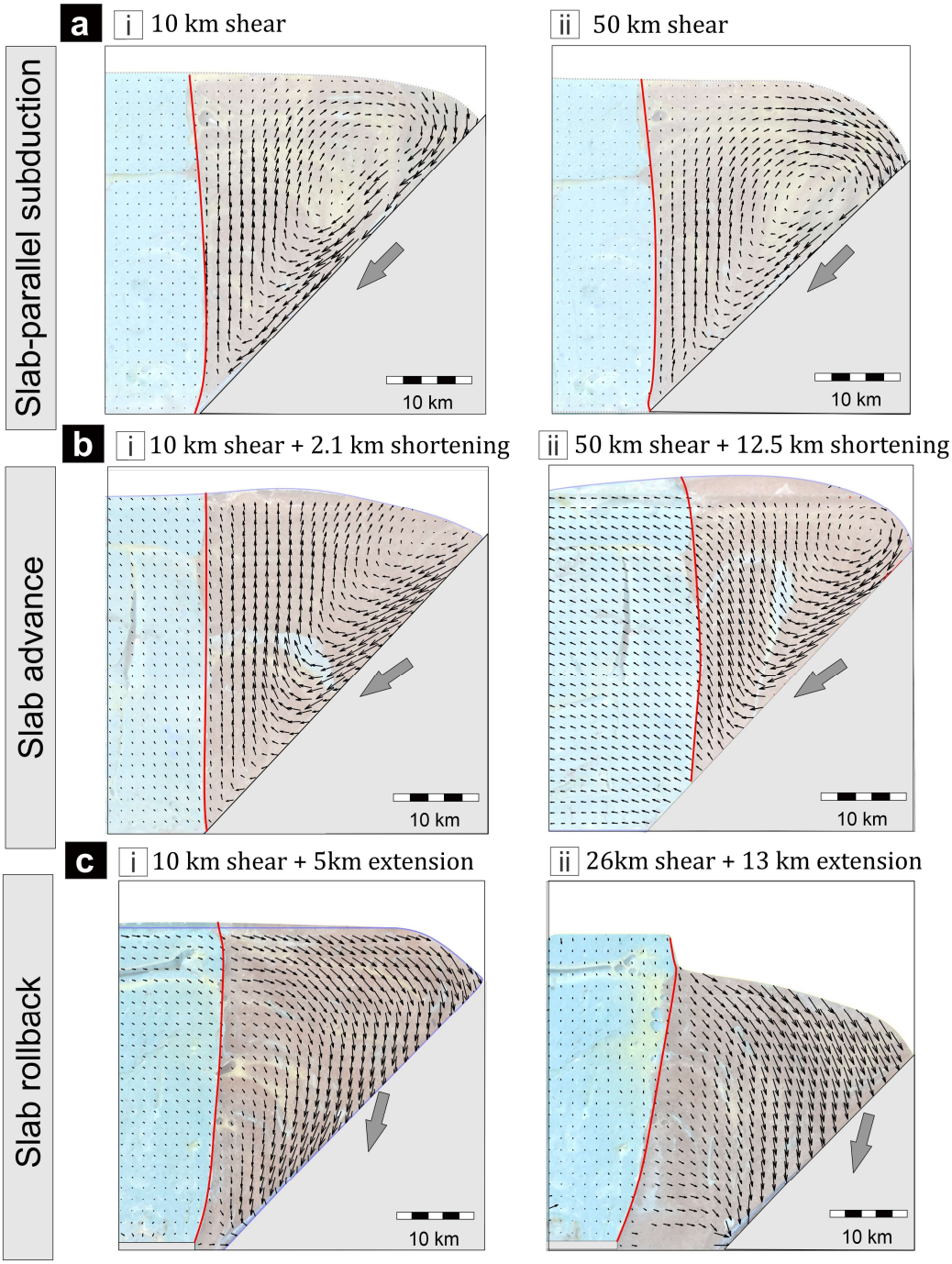

Fig. S3. Evolution of the velocity fields in the whole-model wedges with strong walls ($\mu_r \approx 100$): (a) slab-parallel subduction, (b) slab advance, and (c) slab rollback.

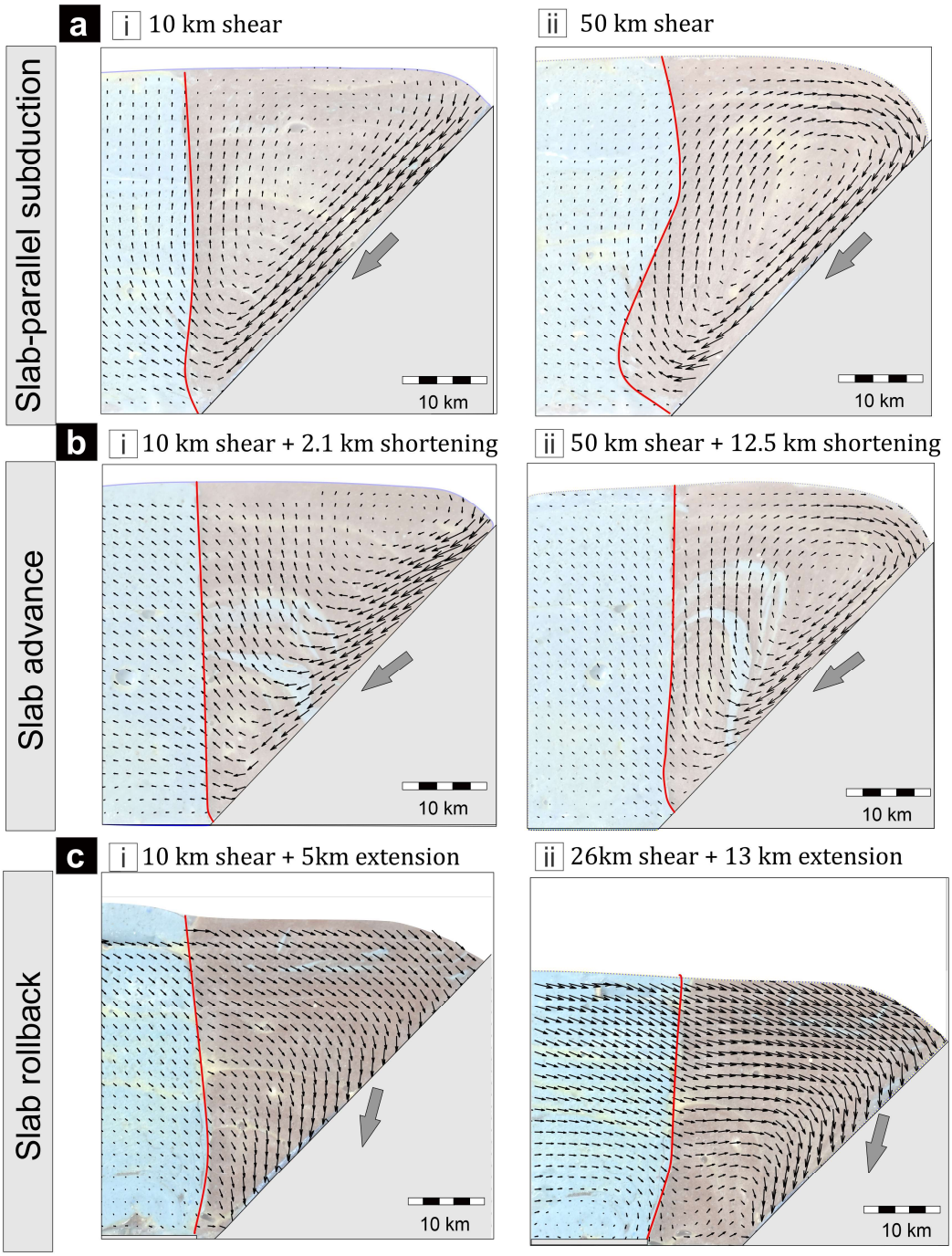

Fig. S4. Evolutions of the velocity fields in the whole-model wedges with weak walls ($\mu_r \approx 10$): (a) slab-parallel subduction, (b) slab advance, and (c) slab rollback.

S5. Upper surface restoration of evolved wedges by material infilling

An additional set of experiment was performed to study the wedge kinematics after finite deformation in absence of any considerable topographic slope. For slab-parallel subduction with low μ_r (≈ 10), the buried wedge materials at an early stage strongly deflect their flow towards the

overriding plate at the bottom 20 km of the wedge (Fig. S5a). These results are in agreement with the analytically predicted velocity field for a wedge with similar settings (Fig. 9a-i in the main text). However, with progressive shear movement, the wedge develops significant topographic slope at the wedge front (Fig. S5b). This results in gravity-driven flow of wedge materials, which forces the return flow vectors to reorient towards the vertical in comparison to the early stages (compare Fig. S5a & b).

After 45 km of shear movement, additional materials were added (equivalent to sedimentation in nature) at the wedge front (Fig. S5b) to restore the wedge upper surface almost horizontal. Experiments show that further shearing results in a velocity pattern similar to that produced in early stages of the experimental run (compare Fig. S5a & c). In absence of any significant topographic slope, the first-order velocity field within the wedge agrees with that predicted from our analytical solutions (section 2, 3 in the main text) over a finite time period.

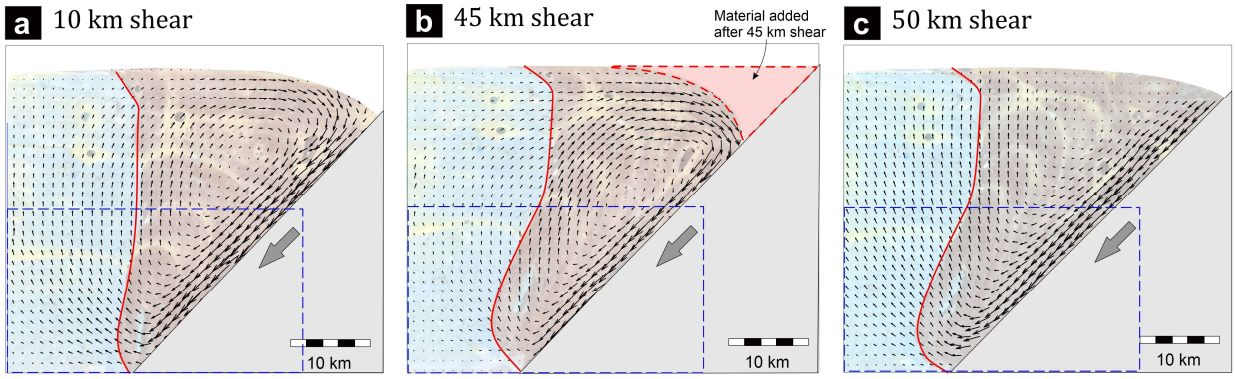

Fig. S5. Laboratory experiments showing the velocity fields in the whole wedge before and after the material infilling in a weak-wall ($\mu_r \approx 10$) model, subjected to slab-parallel subduction. After 45 km of shear, additional material was added to the wedge front, restoring the wedge upper surface almost horizontal. Dashed rectangle (in blue) demarcates the bottom 20 km of the wedge, i.e., the region of interest.